IOP Conf. Series: Earth and Environmental Science **774** (2021) 012067 doi:10.1088/1755-1315/774/1/012067

Opening sequence optimization for La Coche pumps back-to-back start-up through electrically coupled Pelton unit.

Loïc Andolfatto[1], Martin Rentschler[1], Walter Haeussler [2], Nicolas Gervais[1]

[1]Andritz Hydro SA, Rue des Deux-Gares 6, CH-1800 Vevey, Switzerland
[2]Andritz Hydro GmbH, Escher-Wyss-Weg 1, 88212 Ravensburg, Germany

E-mail: loic.andolfatto@andritz.com

Abstract. La Coche pumped storage power plant features 4 pump-turbine units and a Pelton unit, with the possibility for direct full frequency electrical coupling of the Pelton unit generator with the pump turbine motors. The back-to-back start-up mode consists in reaching synchronous speed of both pump unit and turbine unit by using the hydraulic power delivered to the turbine, without requiring absorbed electrical power peak usually perturbing the grid during pump start-up.

The fastest start-up is achieved while the hydraulic power injected in the system is maximized. The associated risk lies in reaching levels of mechanical load of the Pelton runner that dramatically reduce the runner remaining lifetime at each start-up.

The proposed work focus on the Pelton turbine nozzle opening law optimization to minimize the start-up time, while keeping the level of stress in the Pelton runner below a maximum allowed value. Numerical simulations coupling CFD and FEM were associated to train a surrogate model predicting the runner condition along the transient start-up sequence. Resolution of the first order differential equation of the coupled units start-up trajectory under boundary conditions defined from nozzle opening sequence allowed to assess both associated start-up time and stress levels.

Results of the field measurement gathered during the commissioning phase were compared to simulation results to update the implemented model parameters and optimize the start-up sequence allowing fast and long lasting back-to-back start-up capacity.

1. Introduction

Harvesting renewable energy sources is one of the keys to achieve a significant reduction of greenhouse gases emission in the coming decades. Several mature technologies such as photovoltaic panels and wind turbines have already been successfully integrated into large, interconnected, continental-scale electricity supply systems despite their non-dispatchability [1]. Balancing such systems between generation and consumption requires additional capacity for energy storage and operation flexibility that can be provided by pumped storage hydro power plants.

Start-up of the pump requires a peak of power, typically absorbed from the grid, which yields grid perturbation. This could be avoided with the so called back-to-back start-up mode: the pump unit reaches synchronous speed thanks to the power delivered by the turbine unit, itself

started using the hydraulic power delivered by the water flow. The coupling between the pump unit and the turbine unit can be mechanical along a single shaft as for the Veytaux powerplant for example [2] or electrical by connecting the turbine generator and the pump motor as for La Coche powerplant.

La Coche pumped storage power plant features four 5-stages Francis reversible pump-turbine units with rated power of 80 MW commissioned during the 70's and one Pelton turbine unit with rated power of 240 MW commissioned in 2019. A full frequency electrical coupling can be established between the Pelton unit generator and each of the pump-turbine motors.

During the early seconds of the back-to-back start-up, the Pelton unit is operated at a speed close to zero while already converting hydraulic power, with a risk of highly overshooting the mechanical solicitation of the runner normally experienced during continuous operation. This risk is mitigated by limitations on the hydraulic power feeding the system according to an appropriate nozzle opening sequence. Yet, reducing the start-up time offers more flexibility for the plant operation. The work presented in this paper investigates the optimisation of the Pelton unit opening sequence to deliver fast back-to-back start-up while limiting fatigue damage of each start-up.

The model developed to simulate the back-to-back start-up is presented in section 2. An emphasis is put on the strategy proposed to predict stress in the Pelton runner under transient operating conditions. Comparisons between the results from the measurement campaign performed during the commissioning phase of the unit and the simulation results obtained with the proposed model are presented in section 3. Finally, a discussion on the possible optimisation of the opening sequences is proposed in section 4.

2. System modelling

2.1. Hydraulic modelling of the Pelton turbine

During the back-to-back start-up, the turbine unit and the pump unit are driven by the hydraulic power P_h received by the turbine unit, as expressed in (1) where Q is the discharge, H the net head, ρ the water density and g the gravity acceleration.

$$P_\mathrm{h} = \rho \cdot g \cdot Q(H, z_0, S) \cdot H \tag{1}$$

The discharge flowing through the turbine depends on the net head, on the number of active jets z_0 and of the nozzle opening S. The parameters of the discharge law formulated in (2) are linked to the nozzle geometry. A satisfactory agreement with experiment is obtained with $k = 2$.

$$Q(H, z_0, S) = z_0 \cdot \sqrt{2 \cdot g \cdot H} \cdot \sum_{i=1}^{k} \lambda_i \cdot S^i \tag{2}$$

The mechanical power $P_\mathrm{m,t}$ delivered by the Pelton runner to the shaft is related to the hydraulic efficiency η_h as defined in (3).

$$P_\mathrm{m,t} = \rho \cdot g \cdot Q(H, z_0, S) \cdot H \cdot \eta_\mathrm{h}(n_\mathrm{ED}, Q_\mathrm{ED}) \tag{3}$$

The hydraulic efficiency of the prototype turbine is assumed to depend only on the speed factor n_ED and on the discharge factor Q_ED. The speed factor and discharge factor are defined in (4) and (5) respectively, where ω refers to the angular speed of the turbine shaft increasing during start-up, D_1 refers to the runner pitch circle diameter and B_2 refers to the bucket width.

$$n_\mathrm{ED} = \frac{\omega \cdot D_1}{2\pi\sqrt{g \cdot H}} \tag{4}$$

$$Q_{\mathrm{ED}} = \frac{Q/z_0}{{B_2}^2\sqrt{g \cdot H}} \tag{5}$$

An explicit model of the efficiency can be identified either through reduced scale physical model testing [3] or from CFD simulations.

Similarly, a model of the energetic losses in the waterways, following for example (6), can be established to compute the net head according to the gross head H_{g} and the discharge.

$$H = H_{\mathrm{g}} - k_{\mathrm{eq}} \cdot Q^2 \tag{6}$$

Finally, the combination of eq. (1) to eq. (6) allows to express the mechanical power $P_{\mathrm{m,t}}$ delivered by the Pelton runner to the shaft according to the operating conditions defined by the gross head H_{g}, the number of active jets z_0, the nozzle opening S and the shaft angular speed ω.

2.2. Dynamic modelling of the system

The turbine unit shaft balance equation is formulated in (7) where $T_{\mathrm{t,r}}$ the resisting torque on the shaft, $P_{\mathrm{t}\to\mathrm{g}}$ is the power delivered by the shaft to the turbine generator and J_{t} is the inertia of the unit rotating train.

$$J_{\mathrm{t}}\frac{d\omega}{dt} + T_{\mathrm{t,r}}(\omega) + \frac{P_{\mathrm{t}\to\mathrm{g}}}{\omega} = \frac{P_{\mathrm{m,t}}}{\omega} \tag{7}$$

A similar balance is written for the shaft of the pump to be started, with the subscript p referring to the pump quantities and $P_{\mathrm{m}\to\mathrm{p}}$ is the power delivered by the pump motor to the shaft.

$$J_{\mathrm{p}}\frac{d\omega_{\mathrm{p}}}{dt} + T_{\mathrm{p,r}}(\omega_{\mathrm{p}}) = \frac{P_{\mathrm{m}\to\mathrm{p}}}{\omega_p} \tag{8}$$

The number of pairs of poles of the turbine and pump unit are written $z_{\mathrm{p,t}}$ and $z_{\mathrm{p,p}}$ respectively. The electrical coupling between the turbine unit and the pump unit is assumed to ensure synchronous frequencies in the turbine generator and in the pump motor, as expressed in eq. (9). It can be derived into the kinematic coupling defined in (10).

$$z_{\mathrm{p,p}} \cdot \omega_{\mathrm{p}} = z_{\mathrm{p,t}} \cdot \omega \tag{9}$$

$$\omega_{\mathrm{p}} = \frac{z_{\mathrm{p,t}}}{z_{\mathrm{p,p}}}\omega = z_{\mathrm{p,r}} \cdot \omega \tag{10}$$

From the power point of view, the electrical coupling can be modelled according to (11), where the electrical efficiency of the generator and motor are considered.

$$P_{\mathrm{m}\to\mathrm{p}} = \eta_{\mathrm{el,m}} \cdot \eta_{\mathrm{el,g}} \cdot P_{\mathrm{t}\to\mathrm{g}} = \eta_{\mathrm{el}} \cdot P_{\mathrm{t}\to\mathrm{g}} \tag{11}$$

Finally, (7) to (11) can be combined to formulate the differential equation (12) modelling the dynamic system of electrically coupled turbine and pump unit with the rotating speed of the turbine unit ω as a single variable and external forcing conditions depending on the gross head, the number of active jets and the nozzle opening as established in subsection 2.1.

$$\left(J_{\mathrm{t}} + \frac{{z_{\mathrm{p,r}}}^2}{\eta_{\mathrm{el}}}J_{\mathrm{p}}\right)\frac{d\omega}{dt} + T_{\mathrm{t,r}}(\omega) + \frac{z_{\mathrm{p,r}}}{\eta_{\mathrm{el}}}T_{\mathrm{p,r}}(z_{\mathrm{p,r}}\omega) = \frac{P_{\mathrm{m,t}}(H_{\mathrm{g}}, z_0, S)}{\omega} \tag{12}$$

Assuming appropriate models for the resisting torque on the shafts and for the electrical efficiencies of the generator and motors, the start-up trajectory of the system can be simulated by solving the differential equation (12) under any given operating condition of gross head, number of active jets and opening sequence.

The fluid-structure interaction along such transient operating trajectory needs to be studied to evaluate the stress level experienced in the Pelton bucket.

2.3. Stress prediction along a transient operating trajectory

2.3.1. Fluid-Structure interaction numerical simulation In order to predict the stress in the Pelton bucket runner, and especially in the root area, the present paper relies on transient computational fluid dynamics (CFD) simulation to generate the pressure distributions on the Pelton bucket [4]. These pressure fields are extracted from all the CFD simulation time steps for a complete jet passage through a bucket to feed static finite element analysis (FEA) [5].

The stress profile experienced over one cycle of jet passage through a bucket is computed for each node of the finite element model mesh. The mean value σ_{m} of the stress along a cycle together with the peak-to-peak amplitude σ_{pp} characterising the fatigue solicitation of the bucket can be evaluated on the entire bucket geometry.

The relative mean stress and relative peak-to-peak stress are defined in (13) and (14) respectively, according to the admissible stress limits $\sigma_{\mathrm{m,lim}}$ and $\sigma_{\mathrm{pp,lim}}$, which depend on the material of the runner and of the manufacturing method.

$$\sigma^*_{\mathrm{m}} = \frac{\sigma_{\mathrm{m}}}{\sigma_{\mathrm{m,lim}}} \tag{13}$$

$$\sigma^*_{\mathrm{pp}} = \frac{\sigma_{\mathrm{pp}}}{\sigma_{\mathrm{pp,lim}}} \tag{14}$$

This procedure accounting for the complete jet passage through a bucket is valid for steady-state operating conditions. Adaptations are required to predict the stress along a transient operating trajectory.

2.3.2. Stress response surface identification During the start-up, the fluid-structure interaction problem is transient with time-dependant boundary conditions: the rotating speed is the solution of an ordinary differential equation with a solution depending on the nozzle opening law. In order to cope with this difficulty, the following assumptions are made:

- the head variation during the transient period is low and can be neglected;
- the bucket mechanical response dynamics is faster than the operating conditions variation.

Considering these assumptions, each mechanical state reached during the transient start-up is considered to be the same as the one obtained with quasi-static operating conditions fulfilling the similitude of speed factor n_{ED} and discharge factor Q_{ED}.

To cope with the high computing efforts required to perform the transient FSI simulation for numerous investigated start-up scenarios, the strategy proposed in this work relies on a metamodelling approach with response surfaces predicting the stress as bivariate functions of the operating conditions $(n_{\mathrm{ED}}, Q_{\mathrm{ED}})$. Such strategies have been extensively used to solve similar highly-expensive black-box problems [6, 7].

The start-up operating domain is sampled with N pairs of points $(n_{\mathrm{ED}}, Q_{\mathrm{ED}})$ covering a domain including the foreseen investigated start-up trajectories. Then N associated steady-state computationally expensive FSI simulations described in 2.3.1 are run to compute the corresponding mean stress σ_{m} and the peak-to-peak stress σ_{pp} in the bucket root, taken at the point of maximum stress amplitude.

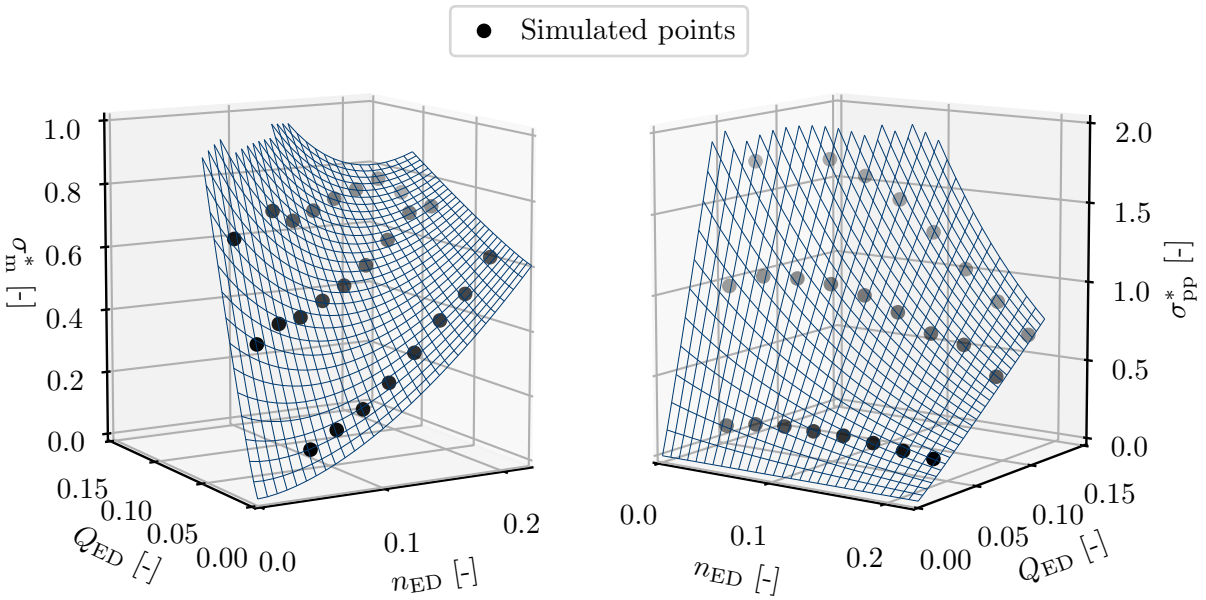

Figure 1. Relative mean stress σ^*_{m} and relative peak-to-peak stress σ^*_{pp} as functions of the speed factor and of the discharge factor, together with the 25 simulated points.

Finally, the parameters of the relative mean stress function σ^*_{m} defined in (15) and the parameters of the relative peak-to-peak stress function σ^*_{pp} defined in (16) are identified based on the N simulation results.

$$\sigma^*_{\mathrm{m}}(n_{\mathrm{ED}}, Q_{\mathrm{ED}}) = \frac{1}{\sigma_{\mathrm{m,lim}}} \cdot \left[k_m \cdot {n_{\mathrm{ED}}}^{n_m} + \left(n_{\mathrm{ED},0_m} - n_{\mathrm{ED}}\right)^{p_m} \cdot {Q_{\mathrm{ED}}}^{q_m}\right] \tag{15}$$

$$\sigma^*_{\mathrm{pp}}(n_{\mathrm{ED}}, Q_{\mathrm{ED}}) = \frac{1}{\sigma_{\mathrm{pp,lim}}} \cdot \left(n_{\mathrm{ED},0_{pp}} - n_{\mathrm{ED}}\right)^{p_{pp}} \cdot {Q_{\mathrm{ED}}}^{q_{pp}} \tag{16}$$

The mean deviation between the response surfaces and the simulation results illustrated in Fig. 1 are 2.1% and 1.5% for the relative mean stress and the relative peak-to-peak stress respectively.

Then, predicting the stress experienced by the Pelton runner along a transient trajectory with time-dependent boundary conditions is limited to the computing efforts to evaluate the response surfaces from eq. (15) and eq. (16). Exploration of multiple start-up sequences and stress-based optimisation becomes achievable without committing further high-performance computing resources.

3. Assessment of the stress prediction

3.1. Experimental setup

During the commissioning of the Pelton unit in La Coche powerplant, several tests including stress measurement on the buckets have been performed. One test focused on the evaluation of the stress during the back-to-back start-up of one pump unit. The start-up was performed with five active jets.

The turbine rotating speed, the static pressure at the turbine distributor inlet and the nozzle opening stroke were recorded from the turbine governing system. Together with the discharge

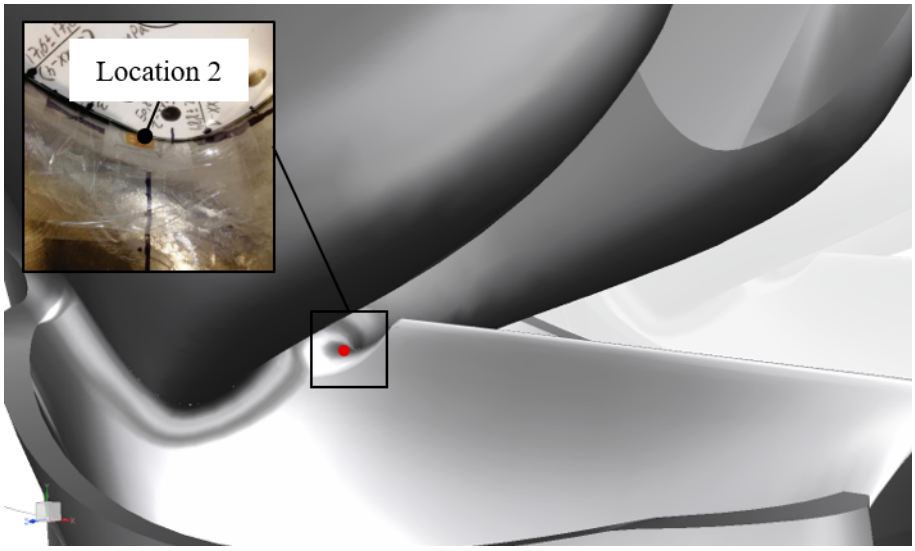

Figure 2. Location of the strain gauges B7.2, B15.2 and B16.2 at the root of buckets.

law of the nozzle presented in 2.1, this allows to evaluate the evolution of the speed factor n_{ED} and the discharge factor Q_{ED} over time.

Quarter bridge strain gauges have been installed on three buckets numbered B7, B15 and B16 at the location indexed 2 corresponding to the point experiencing the maximum stress amplitude at maximum power and rated head, according to the FSI simulations performed during the development of the runner, as illustrated in Figure 2. This location has been selected to address several goals during the commissioning and not specifically for the purpose of this study. The strain gauge signals are recorded with a sampling frequency of 5 kHz. Mean values and peak-to-peak values (from a coverage interval of 97.5%) of these signals are then computed on windows of 0.15 s.

3.2. Measurements compared to predictions

The $(n_{\mathrm{ED}}, Q_{\mathrm{ED}})$ start-up trajectory is evaluated according to the signal measured from the governing system. The relative mean stress σ^*_{m} and the relative peak-to-peak stress σ^*_{pp} during the start-up are then computed using the response surfaces from (15) and (16) respectively. The predicted values are plotted in Fig. 3 together with the values derived from the strain gauges measurement.

3.3. Discussion about the predictions

The deviation between predicted and measured relative mean stress and relative peak-to-peak stress is evaluated on the time window from 10 s to 65 s to avoid bias from the steady-state conditions at beginning and end of the test. The mean values from the three sensors is compared to the predicted values. Along this window, the relative mean stress is overestimated by 6.8% while the relative peak-to-peak stress is underestimated by 8.4%.

Regarding the overestimation of the relative mean stress, it is partly due to the mismatch between the developed prediction methodology and the possibility for experimental data acquisition. For each of the FSI simulation run result considered to build the response surface, the extracted values is the mean stress at the point of maximum stress amplitude. Instead of always

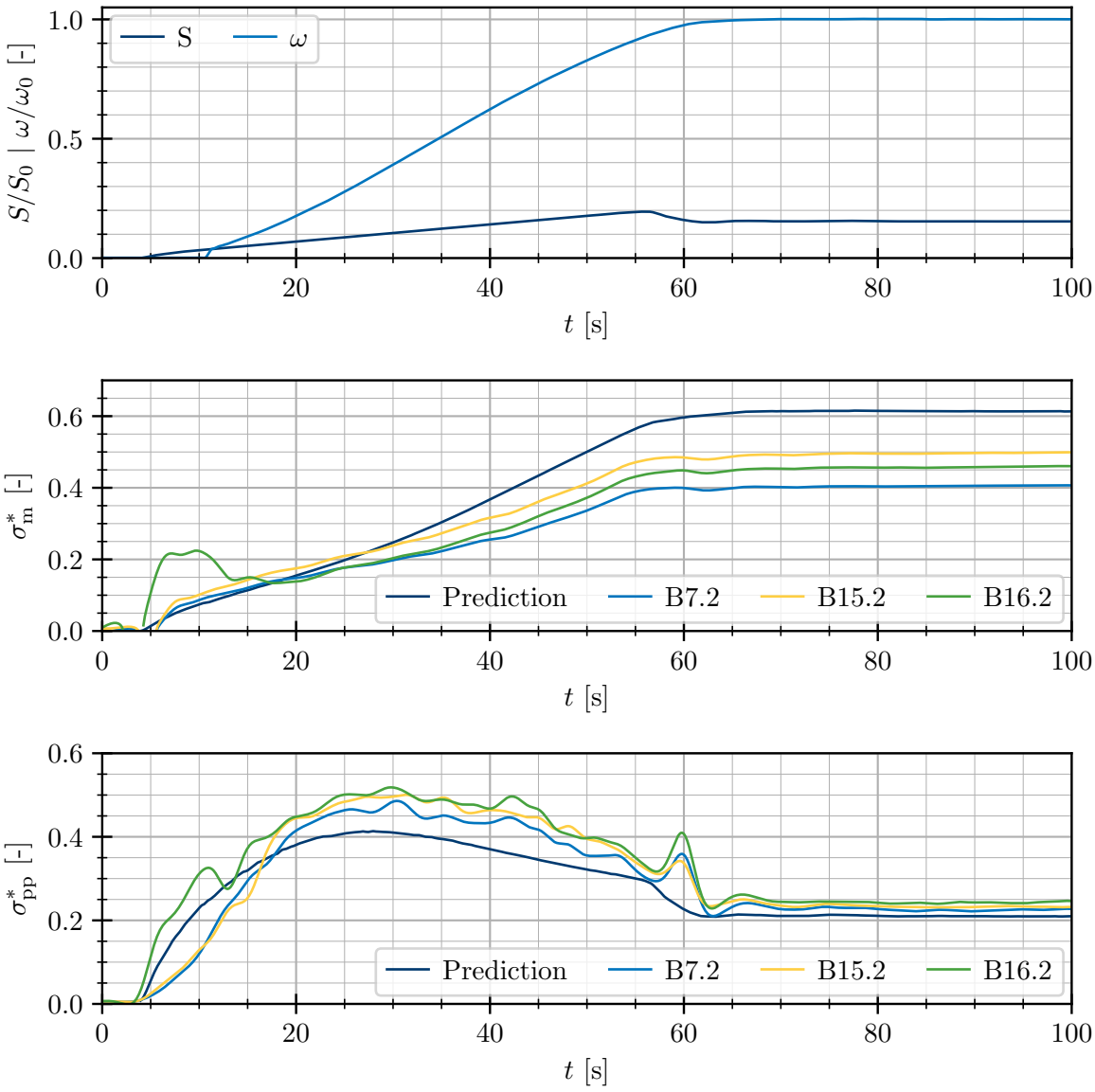

Figure 3. Measurement results compared to the predicted relative mean stress and relative stress amplitude.

being coincident with the location of the installed strain gauge, this point wanders in the bucket root region while the operating conditions vary. Thus, the response surface building procedure is conservative regarding the relative mean stress.

The measured stress is the combination of the bucket response to jet solicitations and to its response to auto-excitation. The analysis of the measured signal spectrum on several time windows during the start-up showed some components corresponding to the natural frequencies of the bucket. This is not accounted for in the FSI simulation which only considers quasi-static mechanical loading of the bucket, therefore leading to underestimated stress amplitude.

Finally, the comparison between the measurement during a start-up sequence and the prediction from the proposed model showed discrepancies of an order of magnitude that is similar to the measurement uncertainty, which is illustrated by the differences between values obtained with the same measuring equipment installed at three different locations of the runner. To conclude, the hypothesis used to develop and implement the procedure described in 2.3.2 to evaluate the stress in the buckets under transient operating conditions at low speed appears to yield realistic results.

4. Opening sequence optimisation

4.1. Evaluation

The ideal opening sequence allows to reach the synchronous speed within the minimum start-up time t_{start} with the minimum usage factor per start-up U for the Pelton runner. The usage factor per start-up U measures the fatigue damage caused by a start-up sequence to the runner. The definition of (17) is derived from Miller law [8], where $\mathcal{N}$ is the number of fatigue cycles until the rupture under the mechanical loading $(\sigma^*_{\text{m}}, \sigma^*_{\text{pp}})$.

$$U = \int_0^{t_{\text{start}}} \frac{1}{\mathcal{N}\left(\sigma^*_{\text{m}}(t), \sigma^*_{\text{pp}}(t)\right)} \cdot z_0 \cdot \frac{\omega(t)}{2\pi}\, dt \tag{17}$$

The design variable of the optimization are related to the opening sequence. The number of active jets is fixed to 5, to lower the mechanical load from each jet. The domain to be explored is limited by the maximum opening speed to avoid surge issues due to transient effects in the waterways. Only monotonous laws, with the needle travelling in the opening direction are considered. Then, the opening sequence is finally defined by pairs of target nozzle opening values and target time.

The differential equation (12) established in subsection 2.2 can be used to predict the transient trajectory of a back-to-back start-up and evaluate the start-up time t_{start} associated to the investigated opening sequence. For La Coche, the dynamic parameters of the pump-turbine unit are identified from the back-to-back start-up tests of one pump-turbine unit in pumping mode with another pump-turbine unit in pump mode [9]. The dynamic parameters of the newly commissioned Pelton turbine unit are taken from commissioning test results. The procedure from subsection 2.3 can be applied to evaluate the mechanical loading of the runner during the start-up.

4.2. Optimisation

The two objectives of minimum start-up time and minimum usage factor conflicts with each other. The result of the optimisation is a Pareto front exhibiting the non-dominated opening sequence, for which no other sequence has been found to yield faster start-up with lower usage factor.

Solving such problems usually requires numerous calls to the performance functions. With the proposed surface response strategy, the evaluation cost of the performance function is several order of magnitude lower than with direct usage of transient FSI simulations. The optimisation problem can be then be solved with methods relying on intensive calls to the performance functions, such as the NSGA II multi objective algorithm [10] implemented in the Inspyred Python library [11] used for this work.

The Pareto front is plotted in Fig. 4, for opening sequences including either one intermediate step (as in Fig. 3) or two intermediate steps between closed nozzle an steady-state opening.

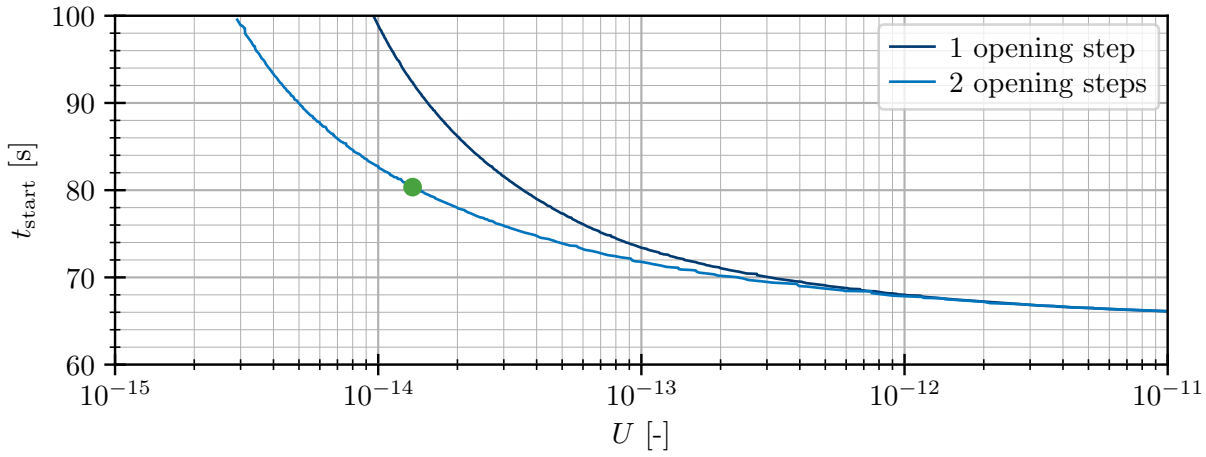

Figure 4. Pareto front showing the start-up time and usage factor of non-dominated opening sequences with 1 intermediate step and 2 intermediate steps.

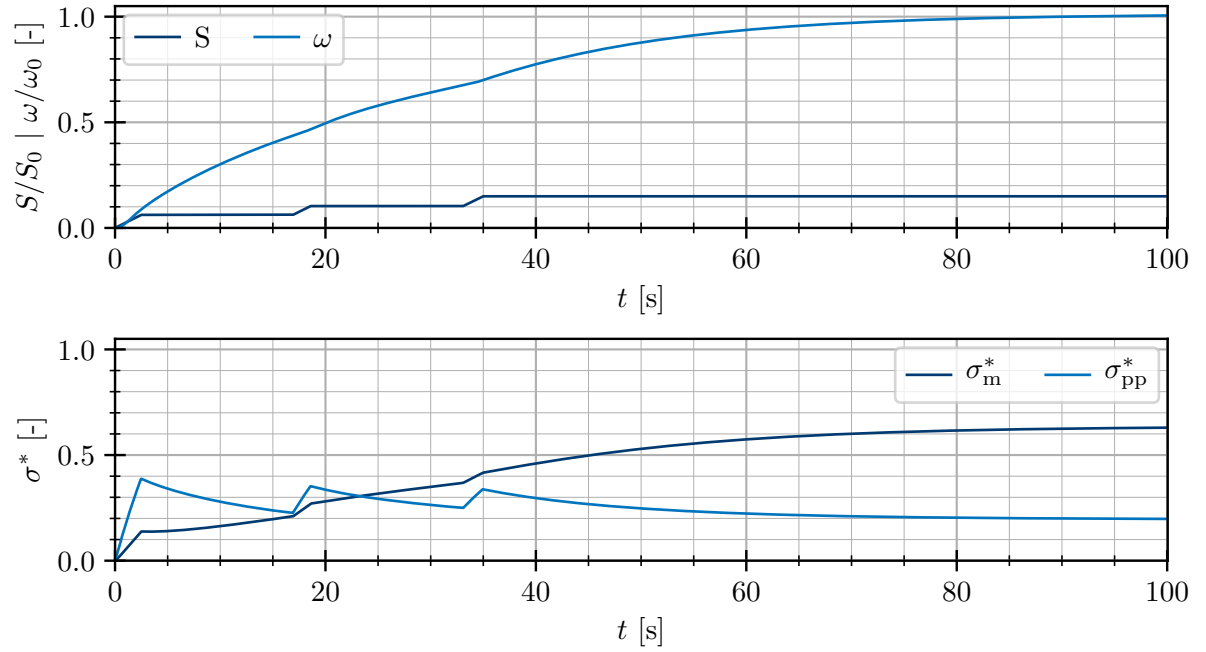

Figure 5. Opening sequence trajectory as highlighted in Fig. 4.

The fastest solution with the most demanding opening sequence regarding fatigue damage correspond to the start-up sequence described in section 3. The graph from Fig. 5 illustrates the opening sequence with two intermediate opening steps and the associated mechanical loading of the highlighted point of the front from Fig. 4.

This example shows that implementing an opening sequence with two intermediate steps could be of interest to reduce the fatigue damage induced on the runner by each back-to-back start-up by a factor 3 with the same start-up time as with one single opening step. It also illustrates the possibility to significantly reduce the usage factor by consenting a slower start-up time.

5. Conclusion

This article aims at presenting a metamodelling approach implemented to support the prediction of the mechanical loading of Pelton runners under transient operation. This overcomes the usual difficulties of computing efforts related to numerical simulations of fluid-structure interactions with time-dependent boundary conditions. Once an initial computational effort has been consented to train the stress response surface with numerical simulation, various scenarios can be evaluated. The commissioning tests of La Coche Pelton turbine gave the opportunity to confront the prediction obtained with the proposed approach to experimental results.

Then, the method has been applied to the optimisation of the back-to-back start-up of La Coche pump unit with the Pelton turbine unit, considering the conflicting objectives of fast start-up and low fatigue damage. This application is only one example of the potential of the proposed method to deliver relevant information to power plant operator and decision makers. Within the context of an electricity market in which the performance is not only related to energy generation but more and more also reflected by unit availability and services to the grid, delivering tools to determine the best strategy to start, operate, stop and maintain the units is also a key for turbine manufacturers.

6. Acknowledgement

The authors would like to thank EDF and in particular EDF Hydro - Centre d'Ingénierie Hydraulique for their collaboration in this study. All the staff both from EDF and from Andritz Hydro who contributed to La Coche site measurement campaign is also warmly thanks.

Multidisciplinary research activities are always stories with many characters, rich with discussions and exchange of know how. This work was no exception and the help received from Andritz Hydro colleagues was appreciated.

References

[1] IPCC (2011) Renewable Energy Sources and Climate Change Mitigation, Ottmar Edenhofer, Ramón Pichs-Madruga, Youba Sokona, Kristin Seyboth, Patrick Matschoss, Susanne Kadner, Timm Zwickel, Patrick Eickemeier, Gerrit Hansen, Steffen Schloemer, Christoph von Stechow (Eds.)

[2] C. Nicolet, A. Béguin, J.-D. Dayer and G. Micoulet (2019) Hydraulic transient challenges for the upgrade of FMHL+ pumped storage power plant from 240MW to 420MW, IOP Conf. Ser.: Earth Environ. Sci. 240 052026, https://doi.org/10.1088/1755-1315/240/5/052026

[3] J.G. Pereira Jr., L. Andolfatto, F. Avellan (2018) Monitoring a Francis turbine operating conditions, Flow Measurement and Instrumentation 63, https://doi.org/10.1016/j.flowmeasinst.2018.07.007

[4] J.C. Marongiu, F. Leboeuf, J. Caro, E. Parkinson (2010), Free surface flow simulations in Pelton turbines using an hybrid SPH-ALE method, Journal of Hydraulic Research, 48:1, https://doi.org/10.1080/00221686.2010.9641244

[5] J.C. Marongiu, E. Parkinson, S. Lais, F. Leboeuf, J. Leduc (2010) Application of SPH-ALE method to Pelton hydraulic turbines, 5th International SPHERIC Workshop, Manchester, UK.

[6] S. Shan, G. Wang (2010) Survey of modeling and optimization strategies to solve high-dimensional design problems with computationally-expensive black-box functions. Structural and Multidisciplinary Optimization, https://doi.org/10.1007/s00158-009-0420-2

[7] C. Vessaz, L. Andolfatto, F. Avellan, C. Tournier (2017) Toward design optimization of a Pelton turbine runner, Structural and Multidisciplinary Optimization 55: 37. https://doi.org/10.1007/s00158-016-1465-7

[8] K.J. Miller (1985) Initiation and Growth Rates of Short Fatigue Cracks, in: Fundamentals of Deformation and Fracture, Eshelby Memorial Symposium, Cambridge University Press, Cambridge, U.K., pp. 477–500.

[9] EDF (2000) Centrale de La Coche - Groupe 03 et 04, Essais de démarrage dos à dos, Internal report.

[10] K. Deb, A. Pratap, S. Agarwal, T. Meyarivan (2002) A fast and elitist multiobjective genetic algorithm: NSGA-II, in IEEE Transactions on Evolutionary Computation, vol. 6, no. 2, pp. 182-197, https://doi.org/10.1109/4235.996017

[11] Garrett, A. (2014). inspyred: Bio-inspired Algorithms in Python. URL: https://pypi. python. org/pypi/inspyred (visited on 15/01/2020).